Probing the role of proton cross-shell excitations in ^{70}Ni using nucleon knockout reactions

B. Elman,[1,2] A. Gade,[1,2] R. V. F. Janssens,[3] A. D. Ayangeakaa,[4] D. Bazin,[1,2] J. Belarge,[1] P. C. Bender,[1,*] B. A. Brown,[1,2] C. M. Campbell,[5] M. P. Carpenter,[6] H. L. Crawford,[5] B. P. Crider,[1,†] P. Fallon,[5] A. M. Forney,[7] J. Harker,[6,7] S. N. Liddick,[1,8] B. Longfellow,[1,2] E. Lunderberg,[1,2] C. J. Prokop,[1,8] J. Sethi,[7] R. Taniuchi,[5,9,10,‡] W. B. Walters,[7] D. Weisshaar,[1] and S. Zhu[6,§]

[1]*National Superconducting Cyclotron Laboratory, Michigan State University, East Lansing, Michigan 48824, USA*
[2]*Department of Physics and Astronomy, Michigan State University, East Lansing, Michigan 48824, USA*
[3]*Department of Physics and Astronomy, University of North Carolina at Chapel Hill, Chapel Hill, North Carolina 27599, USA, and Triangle Universities Nuclear Laboratory, Duke University, Durham, North Carolina 27708, USA*
[4]*United States Naval Academy, Annapolis, Maryland, 21402, USA*
[5]*Nuclear Science Division, Lawrence Berkeley National Laboratory, Berkeley, California 94720, USA*
[6]*Physics Division, Argonne National Laboratory, Argonne, Illinois 60439, USA*
[7]*Department of Chemistry, University of Maryland, College Park, Maryland 20742, USA*
[8]*Department of Chemistry, Michigan State University, East Lansing, Michigan 48824, USA*
[9]*Department of Physics, University of Tokyo, Hongo, Bunkyo, Tokyo 113-0033, Japan*
[10]*RIKEN Nishina Center, 2-1 Hirosawa, Wako, Saitama 351-0198, Japan*

(Received 28 May 2019; published 18 September 2019)

The neutron-rich Ni isotopes have attracted attention in recent years because of the occurrence of shape or configuration coexistence. We report on the difference in population of excited final states in ^{70}Ni following γ-ray tagged one-proton, one-neutron, and two-proton knockout from ^{71}Cu, ^{71}Ni, and ^{72}Zn rare-isotope beams, respectively. Using variations observed in the relative transition intensities, signaling the changed population of specific final states in the different reactions, the role of neutron and proton configurations in excited states of ^{70}Ni is probed schematically, with the goal of identifying those that carry, as leading configuration, proton excitations across the $Z = 28$ shell closure. Such states are suggested in the literature to form a collective structure associated with prolate deformation. Adding to the body of knowledge for ^{70}Ni, 29 new transitions are reported, of which 15 are placed in its level scheme.

DOI: 10.1103/PhysRevC.100.034317

I. INTRODUCTION

Since its first production 30 years ago in neutron-induced fission of ^{235}U [1], the neutron-rich nucleus ^{70}Ni has been the subject of continued experimental and theoretical efforts because of its importance for guiding nuclear structure models along the benchmark proton-magic Ni isotopic chain [2–7] as well as for low-entropy *r*-process nucleosynthesis contributing to the $A \approx 80$ abundance peak [8–11]. From the nuclear structure perspective, ^{70}Ni displays a number of interesting phenomena such as the presence of low-lying electric dipole strength [7] and shape coexistence [2,4,6]. Shape coexistence, indeed, appears to emerge as a common feature in the neutron-rich Ni isotopes, as evidenced by recent work on ^{66,68,70}Ni [2–4,6,12,13] and predictions for ^{78}Ni [14,15]. The energetics and properties of the coexisting structures provide invaluable information on proton and neutron cross-shell excitations overcoming the relevant (sub)shell gaps [2,14,16].

The neutron-rich Ni isotopes highlight the drastic effects of shell evolution that can occur when adding or removing only a few nucleons within an isotopic chain. In ^{68}Ni, there are three known 0^+ states associated with different shapes [2,4,12]: the spherical ground state, an oblate deformed level at 1604 keV, and a prolate deformed one at 2511 keV. In ^{70}Ni, the ground state is predicted to be slightly oblate [2] and a candidate for the expected prolate deformed (0_2^+) level has been reported recently from β-decay studies [6]. Monte Carlo shell-model calculations by Tsunoda *et al.* [2] predicted this prolate minimum to be considerably deeper in ^{70}Ni than in ^{68}Ni. The proposed (0_2^+) level was tentatively established at 1567 keV [6], indeed considerably below the proposed prolate state at 2511 keV excitation energy in ^{68}Ni [3,4].

In general, it is interesting to explore the (band) structures built on top of shape-coexisting 0^+ states as they may provide insights into the nature of the excitations involved; i.e., whether they are associated with deformation and, possibly, collective rotation. In ^{70}Ni, shell-model calculations were only able to reproduce the proposed 2_2^+ state at 1868 keV, which was suggested to feed the (0_2^+) level [6], when proton excitations across the $Z = 28$ shell closure were included in the model space [3]. The deformed structures in ^{70}Ni have

*Present address: Department of Physics, University of Massachusetts Lowell, Lowell, Massachusetts 01854, USA.
†Present address: Department of Physics and Astronomy, Mississippi State University, Mississippi State, Mississippi 39762, USA.
‡Present address: Department of Physics, University of York, York YO10 5DD, United Kingdom.
§Present address: National Nuclear Data Center, Brookhaven National Laboratory, Upton, New York 11973-5000, USA.

also been discussed within the Nilsson scheme in Ref. [5]. Through the β feeding observed in the ^{70}Co $\rightarrow$ ^{70}Ni decay, a connection was made between the prolate states suggested by the shell model in ^{70}Ni and the deformed $1/2^-$ proton intruder state of ^{67}Co with a proposed $1/2^-[321]$ Nilsson configuration [17] and the ^{70}Co$(1^+, 2^+)$ ground state, potentially arising from the coupling of this specific proton configuration with a $1/2^-[301]$ neutron. The strong β feeding of the 2_2^+ state in ^{70}Ni from the ^{70}Co ground state was then conjectured to be an indicator that the two states carry a similar deformation [5].

Such emerging, likely deformed, intruder configurations may result in band structures that would provide stringent tests for nuclear models as they require large configuration spaces and the inclusion of cross-shell excitations. Two-proton knockout from neutron-rich nuclei has been used in the past to selectively probe cross-shell proton excitations in proton-magic nuclei [18].

Here, results are reported from three different measurements that use complementary one-proton, one-neutron, and two-proton nucleon knockout reactions to populate excited states in ^{70}Ni. These different reactions enable the identification of dominant proton and neutron configurations in the wave functions of excited states. Although it is impossible to directly observe the de-excitation from the (0_2^+) level with in-beam γ-ray spectroscopy at 40% of the speed of light, because of the state's long mean lifetime of $\tau(0_2^+) = 2.38^{+0.43}_{-0.36}$ ns [4], evidence against some previously proposed candidates for the $2_2^+ \rightarrow 0_2^+$ transition [3] is provided. In addition, 15 new transitions are placed in the level scheme, and the role of excitations across the $Z = 28$ gap in forming the predicted prolate deformed structure built on top of the 0_2^+ state of ^{70}Ni is explored. It is important to note that the suspected prolate shape in ^{70}Ni is interpreted as such based solely on the aforementioned shell-model calculations [2], where it is understood as resulting from a dominant proton particle-hole configuration. This shape cannot be directly inferred from the present data.

We note that the approach of exploiting complementary nucleon-subtracting or nucleon-adding direct reactions to disentangle the proton and neutron character and particle-hole content of final states has been used widely across the nuclear chart, for example, with γ-ray tagging, in the ^{208}Pb region [19], and, most recently, in the $N = 20$ and 28 islands of inversion [20,21] to probe shell evolution.

II. EXPERIMENT

The measurements were performed at the National Superconducting Cyclotron Laboratory [22] at Michigan State University. The secondary beams of ^{71}Cu, ^{71}Ni, and ^{72}Zn were produced from projectile fragmentation of a ^{76}Ge beam, accelerated by the K500 and K1200 coupled cyclotrons to 130 MeV per nucleon. The primary beam impinged on a 399-mg/cm^2-thick ^{9}Be production target. An aluminum wedge degrader with an areal density of 300 mg/cm^2, located at the midacceptance position of the A1900 fragment separator [23], was used to select the fragments of interest within the three different secondary beam cocktails. The identification of the secondary beam components of interest was accomplished using time-of-flight differences. The secondary beams interacted with the reaction target at energies of 80.2, 82.6, and 76.5 MeV/nucleon for the ^{71}Cu, ^{71}Ni, and ^{72}Zn projectiles, respectively.

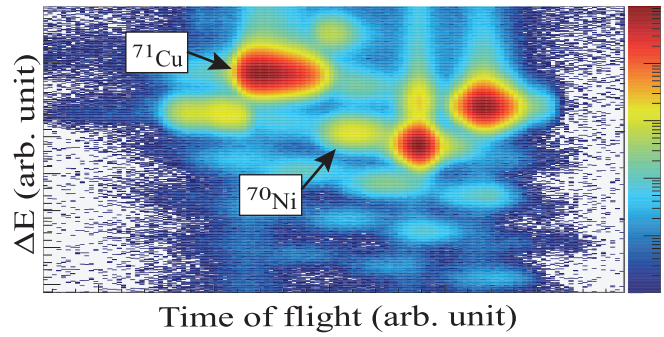

FIG. 1. Particle identification plot (energy loss vs time of flight) for the setting centered on the one-proton knockout from ^{71}Cu. The beam components and different reaction products are identifiable and were cleanly separated with additional software gates on angles and position information in the focal plane.

Two ^{9}Be reaction targets were used during this experiment: one with an areal density of 100 mg/cm^2 for the one-proton knockout reaction and another of 188 mg/cm^2 thickness for the one-neutron and two-proton knockout reactions. For each setting, the target was located at the reaction target position of the S800 spectrograph [24]. The event-by-event identification of the reaction residues and the trajectory reconstruction utilized the detection system of the spectrograph's focal plane, consisting of an ionization chamber, two xy-position-sensitive cathode-readout drift chambers (CRDCs), and a plastic timing scintillator that also served as the particle trigger [25].

An example of the identification of the reaction products emerging from the ^{9}Be target for the ^{71}Cu one-proton knockout setting is given in Fig. 1, where the energy loss measured with the S800 ionization chamber is displayed versus the ion's trajectory-corrected time of flight measured between two plastic scintillators. The ^{70}Ni knockout residues can be separated from the other reaction products, primarily Zn, Cu, Ni, Co, and Fe isotopes. Additional gates on angles and positions in the focal plane were used to remove any contamination by the tails of neighboring nuclei. The identification of the ^{70}Ni residues in the one-neutron and two-proton knockout settings proceeded in the same way.

The Be reaction target was surrounded by the Gamma-Ray Energy Tracking In-beam Nuclear Array (GRETINA) [26], an array of 36-fold segmented high-purity germanium crystals used for in-flight γ-ray detection. At the time of the experiment, the array was composed of nine modules that housed four detectors each in a common cryostat. GRETINA's spatial resolution through signal decomposition provided event-by-event Doppler-reconstruction capability for γ rays emitted in flight [27]. This Doppler correction takes into account the reconstructed trajectory and kinetic energy of each particle at the S800 target position, in addition to the γ-ray interaction points provided by GRETINA.

After passing the scintillator used for the particle trigger, the beamlike reaction residues were implanted in an aluminum plate in front of a CsI(Na) hodoscope array [28], which was arranged in the IsoTagger configuration [29]. This configuration enabled the identification of long-lived states with lifetimes between 100 ns and several ms, such as the 2861-keV level ($\tau = 335(1)$ ns [30]) in ^{70}Ni.

Both ^{71}Cu and ^{71}Ni projectiles exhibit isomers in their level schemes that affect the population of excited states in ^{70}Ni, if present in the beam. In contrast, ^{72}Zn has no known long-lived state. The isomeric content of the beams was measured by placing a 5.1-mm-thick Al stopper at the target position of the S800 spectrograph and measuring the presence of isomeric states with GRETINA through their characteristic γ-ray transitions. In the case of ^{71}Cu, there is a known $(19/2^-)$ state at 2756 keV with a mean lifetime of $\tau = 391(20)$ ns [30]. The isomeric content in the ^{71}Cu beam was determined to be 0.47(7)%, based on the detection of the 133-keV γ ray from this state.

In the case of ^{71}Ni, estimating the isomeric content is more challenging because the long-lived state does not decay directly by γ-ray emission. Instead, the $(1/2^-)$ state at 499 keV with a mean lifetime of $\tau = 3.3(4)$ s [30] in ^{71}Ni undergoes β decay into either the $3/2^{(-)}$ ground state or the 454-keV $(1/2^-)$ excited level of ^{71}Cu [31]. At present, only a 40% upper limit is available for the adopted value for the branching ratio to this 454-keV state in β decay [30]. As a result, based on the intensity of the 454-keV $(1/2^-) \rightarrow 3/2^{(-)}$ transition, a limit of $I_c > 6\%$ was derived for the ^{71}Ni isomeric content.

III. METHODOLOGY AND RESULTS

In the direct one- or two-nucleon nucleon knockout reactions used here, the projectile of interest impinges on a ^{9}Be target, and one or two nucleons are removed, leaving the projectile-like residue as a spectator to the sudden collision [32]. These reactions are often used to quantify spectroscopic strength and probe shell-model spectroscopic factors or two-nucleon amplitudes. However, due to knockout from isomers that cannot be quantified event by event, as well as to (1) mostly unknown or tentative final-state quantum numbers, (2) complex associated configurations, and (3) expected high level densities (see, for example, Ref. [33]), the experiment was optimized for in-beam γ-ray spectroscopy [34]. Hence, γ-ray intensities per reaction residue will be compared across the different reaction channels to assess changes in population of final states rather than to obtain absolute cross sections.

Intensities of emitted γ rays were determined for all three reactions. Uncertainties on these intensities are composed of statistical ones, as well as contributions from the efficiency determination (2.1%) [27] and a specific uncertainty for each separate peak determined from fitting the spectra while varying the fit template and background model. A systematic energy uncertainty of 2.2 keV was determined by comparing observed peak energies with those adopted from the National Nuclear Data Center (NNDC) database [30]. It was added in quadrature with the uncertainty determined from fitting the peaks. Because of the position sensitivity of GRETINA and the emission of γ rays in flight, excited-state lifetimes

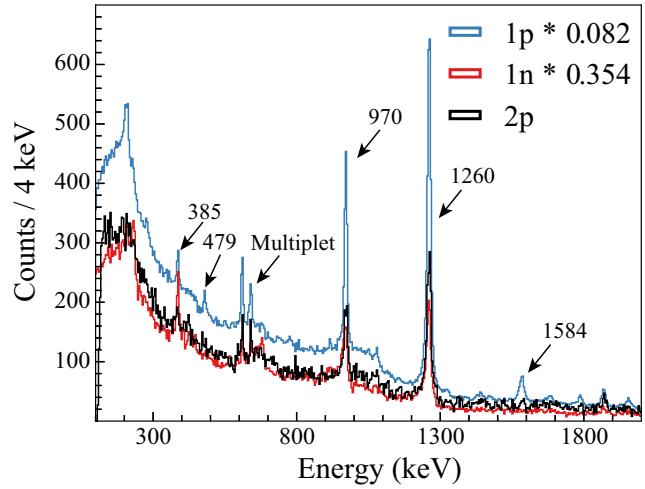

FIG. 2. Comparison of spectra from all three knockout reactions. The one-proton and one-neutron knockout spectra are scaled down by the ratio of the number of ^{70}Ni residues in the focal plane for the specific reaction channel to those detected in the lower statistics two-proton knockout. These scaling factors are given in the figure.

on the order of 10 ps or longer will displace peaks to lower Doppler-reconstructed energies than their actual value. This is not reflected in the energy uncertainties quoted here.

The energy-dependent photopeak efficiency of the setup was determined [27] using standard calibration sources. For the in-beam response of the array, the Lorentz boost of the emitted γ-ray distribution was taken into account via GEANT4 simulations [35]. All intensities were determined using γ-ray singles spectra (see Fig. 2). Levels were placed into the level scheme based on their $\gamma\gamma$ coincidence relationships, taking advantage of nearest-neighbor addback routines for GRETINA [27].

The results for the measured intensities relative to the number of ^{70}Ni residues detected for each reaction channel are summarized in Table I. No feeding subtraction was applied to the quoted intensities, in contrast to the feeding-subtracted state populations discussed in Sec. IV. Note that the fit to extract the intensities included all observed peaks as well as a background model, consisting of both an exponential component (used to model the prompt, beam-correlated background) and stopped lines from annihilation radiation and inelastic reactions of neutrons and other light particles within the germanium crystals or the aluminum beam pipe [36]. The results for placements in the level scheme are given in Fig. 3. Twenty-nine new transitions were observed, of which 15 were placed within the level scheme.

In Fig. 2, the spectra from the one-proton and one-neutron knockout reactions are normalized relative to the two-proton one (see caption for details). The spectra from the three knockout reactions clearly display differences in the population of excited final states. The largest differences are the intensity of the 385-keV transition, whose relative intensity (see Table I) in one-neutron knockout is a factor of 2 larger than in proton knockout, a number of transitions which appear uniquely in proton knockout, such as the 1584- and 479-keV γ rays, and

TABLE I. Measured intensities for all observed ^{70}Ni transitions relative to the number of detected ^{70}Ni residues in the specific reaction channel expressed as a percentage. The error includes both statistical uncertainties and systematic contributions from varying the fit assumption for peak shapes and backgrounds, and a 2.1% uncertainty from the efficiency determination. Note that no feeding subtraction is included here.

State energy (keV)	Transition energy (keV)	Relative intensities (%) $1p$ knockout	Relative intensities (%) $1n$ knockout	Relative intensities (%) $2p$ knockout
1260(2)	1260(2)	44(2)	14.5(8)	21(1)
1868(2)	609(2)	3.6(4)	1.9(3)	2.4(4)
	1868(2)	3.5(6)	1.3(5)	2.5(5)
2230(3)	970(2)	16.5(9)	5.7(7)	7.8(8)
2509(4)	279(3)[a]	0.5(2)	0.3(2)	0.5(2)
	640(2)	2.2(3)	1.2(6)	2.2(4)
	1249(3)[b]	2.4(4)	1.7(3)	1.0(6)
2912(4)	234(4)[c]	0.4(1)	1.5(4)	0.6(2)
	682(3)[d]	1.1(3)	3.9(6)	1.6(5)
2942(4)	1682(3)	1.3(3)		1.0(9)
3215(4)	1955(3)	2.1(2)	0.8(3)	0.7(5)
3297(5)	385(3)	1.3(2)	2.6(7)	1.3(5)
3551(5)	1321(4)	0.7(1)		
3588(6)	676(4)	0.12(3)		0.16(5)
3662(4)	2402(3)	0.8(2)		
	1432(4)	0.3(2)		
3814(3)	1584(2)	4.4(4)		
3846(5)	3846(5)[e]	0.7(1)		
3961(4)	2701(3)	1.6(3)		
4017(4)	1787(3)	1.8(6)		
	2757(3)	1.4(2)		
4293(4)	479(3)	0.7(2)		
	631(4)	0.9(2)		
	2063(3)	0.75(16)		
	3033(5)	1.2(2)		
Unplaced	424(5)		0.6(3)	0.7(3)
	660(3)	0.6(4)	1.2(11)	1.2(4)
	714(4)			1.4(9)
	915(5)	0.9(3)	1.5(4)	
	930(5)	0.33(25)	0.9(3)	
	958(5)	0.6(3)	1.8(5)	
	1212(5)			1.1(5)
	1225(5)		1.7(4)	
	1440(3)	0.8(3)		
	1467(3)	0.5(2)		
	2026(3)	1.2(2)		2.2(5)
	2114(3)	0.8(2)	0.6(3)	
	2342(5)	0.5(2)		
	2980(4)	0.4(3)		

[a]The expected intensity for the 279-keV transition is below the detection sensitivity in the one-neutron and two-proton reaction channels, so the intensity for these reaction channels was estimated based on the branching ratio measured in one-proton knockout.

[b]The discrepancy between the different measurements of the 1249-keV transition intensity relative to the 640-keV one is due both to the difficulty of determining the intensity in a self-coincident doublet and to possible lifetime effects as discussed in Sec. III B. The measured intensities are too small to observe this transition in coincidence with the 1260-keV γ ray in the one-neutron and two-proton reactions.

[c]The intensities given for the 234-keV γ ray for the one-proton and two-proton knockout are determined based on the NNDC adopted branching ratio [30].

[d]The splitting between the self-coincident 676-682 keV doublet is determined based on add-back coincidences for the one-proton knockout. This splitting was then used for the two-proton knockout as well.

[e]The peak is a little wider than expected and the energy was deduced based on the assumption of a single peak; the resulting energy is in agreement with [41].

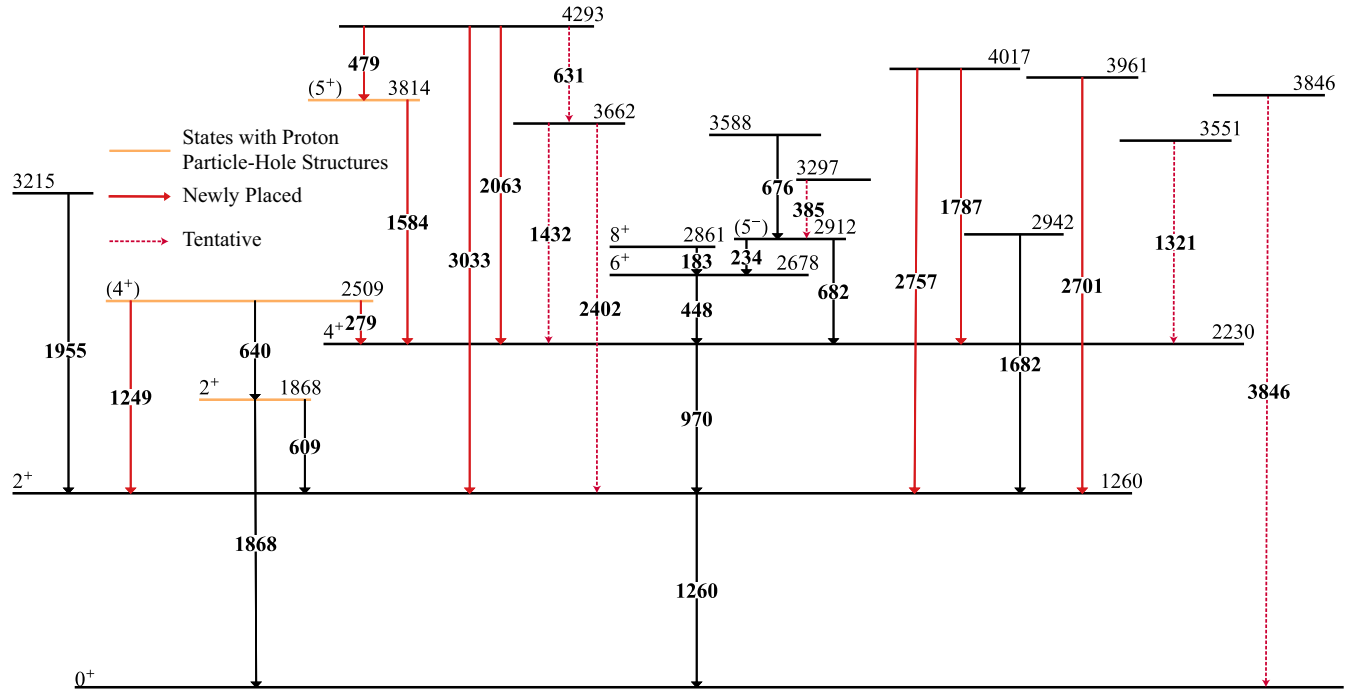

FIG. 3. Proposed ^{70}Ni level scheme containing all the transitions observed in the present measurements. Red arrows indicate newly placed transitions and dashed red ones mark tentative placements. The states highlighted in orange are those associated with proposed proton particle-hole configurations (see text).

the shape of the multiplet between 600 and 700 keV, which varies in all the reaction channels, indicating that some components in the structure change intensity, depending on the reaction. The wide feature near 200 keV that appeared only in the one-proton knockout exhibited no clear coincidence relationships with other transitions, likely because it is in a region of the spectrum where the peak-to-background ratio is poor. Nevertheless, it seems likely that there is more than one transition in the region between 100 and 200 keV, forming the structure visible in Fig. 2. We note that, due to the high detection efficiency at low γ-ray energies, the intensities of such transitions on top of the high background would actually be small.

In the following subsections, each reaction is discussed separately with a main focus on differences between the three channels. For the discussions of single-particle configurations, we remind the reader that (i) one-proton knockout from the dominant $f_{7/2}$ or $p_{3/2}$ orbitals of ^{71}Cu populates positive-parity final states in ^{70}Ni (the ground-state neutron occupations for ^{71}Cu in the shell model with the jj44 interaction are 8.0, 0.06, 0.87, 0.05, and 0.03 for the $f_{7/2}$, $f_{5/2}$, $p_{3/2}$, $p_{1/2}$, and $g_{9/2}$ states, respectively), with negative-parity states originating from the knockout of a *sd*-shell proton expected only at about 7 MeV [37] and that (ii) one-neutron knockout from the $f_{5/2}$, $p_{3/2}$, and $p_{1/2}$ orbitals in ^{71}Ni leads to positive-parity states in ^{70}Ni, while removal of a $g_{9/2}$ neutron populates negative-parity states.

A. One-proton knockout from ^{71}Cu

In the one-proton knockout reaction, states in the yrast band and in the proposed prolate structure were populated more strongly than other levels. Within the latter structure, two new transitions were observed de-exciting the (4_2^+) state at 2509 keV to the yrast sequence. In addition, several higher lying levels of undetermined spin and parity were populated. These decay primarily into the yrast states. A fit to the spectrum for this reaction channel is presented in Fig. 4.

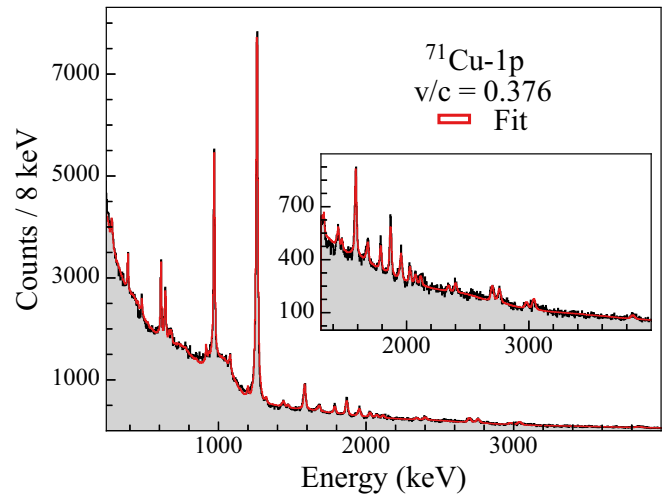

FIG. 4. Fit to the full spectrum of ^{70}Ni obtained in one-proton knockout from ^{71}Cu. This fit includes the simulated response function for all the peaks in the spectrum and a background composed of a double exponential to model the beam-correlated background in addition to stopped background lines from annihilation radiation and inelastic reactions of neutrons and other light particles on the beam pipe or the Ge detectors.

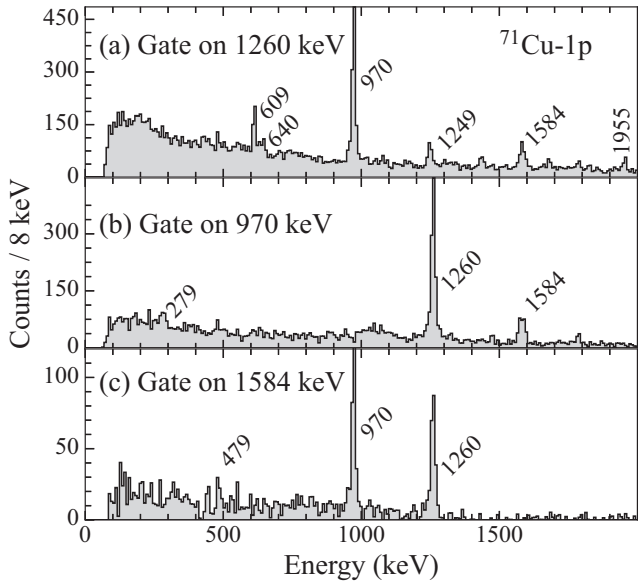

FIG. 5. Coincidence spectrum used to place the 1584-keV transition in the one-proton knockout reaction. Clear coincidence relationships involving the 1260-970-1584 keV transitions allow placing this transition into the level scheme. Also shown in panels (a) and (b) are the two newly placed transitions, 1249 and 279 keV, in what might be the prolate structure.

Twenty-five previously unplaced transitions were observed in this reaction channel, and 15 of these were placed in the level scheme of Fig. 3. Some transitions were difficult or impossible to place due to a combination of low statistics, lack of clear coincidence relationships with known peaks, or insufficient resolution in regions with multiple γ rays close in energy. New transitions originating from the proposed prolate structure are presented in Fig. 5. Specifically, the $(4_2^+) \rightarrow 2_1^+$, 1249-keV γ ray is clearly seen in Fig. 5(a), while the 279-keV, $(4_2^+) \rightarrow 4_1^+$ transition is present in Fig. 5(b). The spin-parity quantum numbers for this (4_2^+), 2509-keV level are tentative as they are based on the observed coincidence relationships with known transitions from the 2_2^+ state as well as on the absence of the 640-keV, $(4_2^+) \rightarrow 2_2^+$ γ ray in β-decay measurements [38,39]. It should be noted that the two new 1249- and 279-keV transitions were not observed in the two-neutron knockout measurement of Ref. [3]. This is possibly due to the former being part of a doublet peak and the latter belonging to a region of the spectrum where the peak-to-background ratio was poor.

The majority of newly placed transitions originate from higher lying states that decay toward the established yrast levels. The strongest of these is the 1584-keV line feeding the 4_1^+, 2230-keV state. Coincidence spectra, instrumental in placing this γ ray, are found in Fig. 5(a), which provides a spectrum coincident with the $2_1^+ \rightarrow 0_1^+$ ground-state transition in which the 1584-keV γ ray is evident. The latter spectrum also displays transitions associated with the proposed prolate structure such as the newly placed 1249-keV γ ray and the previously observed 609- and 640-keV ones. The spectrum in coincidence with the 970-keV transition of Fig. 5(b) documents the placement of the 1584-keV γ ray as feeding the 4_1^+ state from a newly placed 3814-keV level. A placement as populating the 6_1^+ yrast state is ruled out, based on the 1.51(4)-ns lifetime [40] of the latter level prohibiting the observation of coincidence relationships for these fast-moving reaction products. Finally, the spectrum gated on the 1584-keV line itself [Fig. 5(c)] demonstrates the expected presence of the 970–1260-keV, $4_1^+ \rightarrow 2_1^+ \rightarrow 0_1^+$ cascade. The observation of a weak 479-keV γ ray is noteworthy as well, as discussed further below.

As seen in Fig. 3, the 3814-keV state appears to decay only to the 4_1^+ state. Because of the large intensity of the 1584-keV transition feeding the 4_1^+ level, and the available orbitals from which protons can be removed, it is possible that the 3814-keV level is a (5_1^+) state with a $\pi 1p_{3/2}^{+1} 0f_{7/2}^{-1}$ particle-hole configuration. However, these configuration and spin-parity assignments remain tentative.

The 4017- and 4293-keV states are two newly proposed levels that are populated as strongly as the 3814-keV one. As seen in Fig. 3, both exhibit considerably more branching to other states when compared to the 3814-keV state. These decay branches include intense, direct transitions to the 2_1^+ level, which strongly suggests that these states have spin $I \leqslant 4$.

The 4293-keV state's strongest decay branch is to the 2_1^+ state, although there are three somewhat weaker transitions to the (5^+) level (via the aforementioned 479-keV transition), the 4_1^+ one, and a new state at 3662 keV. This suggests a possible spin-parity assignment of $(3^+, 4^+)$. Similar arguments hold for the 3662- and 4017-keV states, but because these have no connection to the 3814-keV, (5^+) level, they can possibly correspond to $(2^+, 3^+, 4^+)$ states. These are most likely of positive parity, considering the available orbitals from which protons can be knocked out. Strong population of negative-parity states would require either indirect, possibly unresolved, feeding from positive-parity levels or knockout of protons from the *sd* shell. Levels populated from the knockout of *sd*-shell protons are only expected to appear starting at energies near 7 MeV in the level scheme [37].

The 1682-keV γ ray reported here possibly corresponds to the 1676-keV transition observed in two recent β-decay experiments [5,6]. It was seen following the β decay of the $(1^+, 2^+)$ state of ^{70}Co and is observed here in both of the proton reaction channels, albeit only weakly in two-proton knockout. The reason for the potential discrepancy between the measured centroids in the different measurements is unclear.

The 1955-keV transition only displays a clear coincidence with the 1260-keV one [see Fig. 5(a)]. This decay out of the 3215-keV level appears in all reaction channels and has also been reported following β decay [5,6] from the $(1^+, 2^+)$ state of ^{70}Co as well as two-neutron knockout [3].

The 3846-keV γ ray was reported previously following the β decay of the low-spin isomer in ^{70}Co, and tentatively placed as feeding the proposed prolate 1868-keV state [41]. This placement cannot be confirmed through coincidence relationships in the present data. Because of the absence of coincidence information, it is tentatively placed here as directly feeding the ground state. This transition was observed

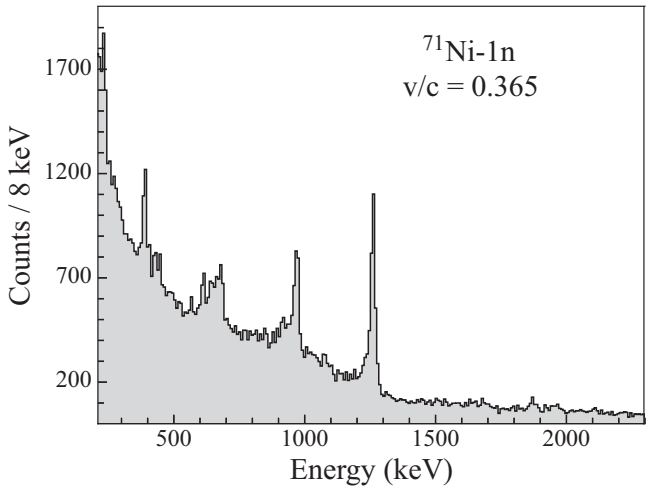

FIG. 6. Doppler-reconstructed γ-ray spectrum in coincidence with the ^{70}Ni knockout residues for the one-neutron knockout from ^{71}Ni.

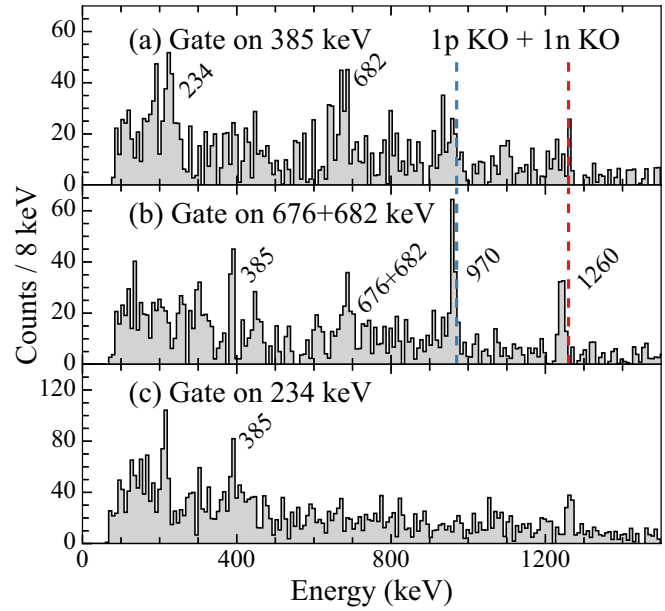

FIG. 7. Coincidence spectra for the 385-keV, the 676–682-keV doublet, and the 234-keV transitions from the sum of the one-proton and one-neutron knockout reaction channels. Because of low statistics, the placement of the 385-keV transition remains tentative. The displacement of the yrast energies in panel (b), as indicated by the dashed lines at the expected yrast energies, is discussed in the text.

almost exclusively in events with a detector multiplicity of 1, herewith supporting this placement. However, the fact that it could decay into the isomeric (0_2^+) state at 1567 keV [6] cannot be ruled out in view of the associated lifetime. It is unlikely to decay into the other known isomers, e.g., the 6_1^+ or 8_1^+ yrast levels, as it was observed in the β decay from a (1^+, 2^+) low-spin state.

As can be seen in the level scheme of Fig. 3, a 682-keV γ ray is placed as de-exciting the proposed [3] 2912-keV, (5^-) level into the 4_1^+, 2230-keV state. In the present experiment, this transition forms an unresolved doublet with a γ ray with a 676-keV approximate energy. The latter has been previously observed following the β decay of the short-lived (6^-, 7^-) state in ^{70}Co [6]. The data indicate that the two components of the doublet are in mutual coincidence and, combining the observations from the literature with those from the present data, leads to the placements proposed in Fig. 3. It should be noted that the direct population of the (5^-) level would require proton removal from the rather deeply bound *sd* shell. As already mentioned, this is viewed as unlikely and, hence, this 2912-keV state is probably fed from higher lying levels.

As discussed above, the observation of γ decay from negative-parity states in the proton-knockout reactions is expected to be the result of feeding by transitions from positive-parity states or high-lying, negative-parity levels populated by proton removal from the *sd* shell. Although the spin and parity of the states which appear coincident with the 234- and 682-keV transitions are unknown, the full intensity of the transitions from the (5^-) level in the proton-knockout channels can be accounted for through feeding of the coincident 676- and 385-keV transitions. The placement of the latter is discussed in the following section.

B. One-neutron knockout from ^{71}Ni

The Doppler-corrected γ-ray spectrum observed for the one-neutron knockout reaction can be found in Fig. 6. This channel exhibits a considerably different final-state population pattern than that observed in both proton knockout reactions. The largest differences observed between the one-neutron and one-proton channels are a decrease in the feeding-subtracted population of states that may be attributed to the proposed prolate structure and an increase in both that of the previously observed (5^-) level and the population of the state decaying via the 385-keV γ ray. The feeding-subtracted state populations are discussed in more detail in Sec. IV. Note that, unlike the proton knockout reactions, the neutron knockout one is expected to directly populate states of negative parity.

The strongest unplaced peak in the spectrum is the previously reported 385-keV transition [3]. It is tentatively placed as de-exciting a 3297-keV state, based on the coincidence relationships with the 682- and 234-keV transitions from the (5^-) state. Figure 7 provides coincidence spectra resulting from the sum of the data for the one-proton and one-neutron reaction channels. The 676-keV transition, observed in coincidence with the 682-keV γ ray depopulating the (5^-) level in the one-proton knockout reaction, is not observed in one-neutron knockout. As the 385-keV line is only weakly populated in the low-statistics two-proton knockout channel, data from the latter reaction were not included in the sum. Relatively weak coincidence relationships among the 385-, 676–682-, and 234-keV transitions can be observed (see Fig. 7).

Aside from the limited statistics in the coincidence spectra, the position of the two peaks near 957 and 1249 keV in coincidence with the 676–682-keV doublet [Fig. 7(b)] also complicated the placement of the 385-keV transition. As shown by the dashed lines in the figure, both yrast transitions

appear to be offset by roughly 13 keV from their expected energies of 970 and 1260 keV, respectively. It is possible that this shift also accounts for the low-energy tails visible for these two γ rays in the Doppler-reconstructed spectrum of Fig. 6. Energy shifts of this type might be due to lifetime effects and some have been observed in previous measurements; e.g., see Ref. [42]. To explore this possibility further, a simulation was carried out for a cascade starting from the 2912-keV (5^-) level and proceeding through the 4_1^+ and 2_1^+ yrast states. The (5^-) level lifetime was varied until energy shifts of the proper magnitude were obtained. To account for the data, a lifetime $\tau(5^-) \geqslant 75$ ps is required.

Displacements in Doppler-corrected energy due to the lifetime of the decaying state can occur both because of the uncertainty in the determination of the particle velocity at the time of γ-ray emission and because the γ decay occurs behind the target. In the former case, long-lived states de-excite at a lower average velocity than prompt transitions, as the nucleus has traversed more of the target material and slowed down relative to prompt midtarget emission. In the latter, the exact emission angle is underestimated as the decay is assumed to take place at midtarget, herewith resulting in a lower transition energy for detectors located at forward angles.

Note that such displacements caused by lifetime effects could potentially account for the presence–or for the partial intensity–of some of the unplaced transitions listed at the bottom of Table I. For example, as already pointed out above, the 957-keV γ ray could originate from the improper Doppler correction of the 970-keV transition. Also, the 1249-keV line was placed within the proposed sequence of prolate levels based on observed coincidence relationships in one-proton knockout, but part of its intensity could conceivably be attributed to the contribution from a long-lived feeding state impacting the 1260-keV transition. Unfortunately, the level of statistics in the one-neutron knockout channel proved insufficient to verify the expected coincidence relationships within the 1249–1260-keV cascade. Furthermore, some of the unplaced γ rays of Table I could be associated with transitions reported in other works, for which a placement in the level scheme of Fig. 3 could not be confirmed because of either the presence of isomeric states or the lack of statistics for the one-neutron knockout data. For example, this may be the case for the 915-keV line seen in the present work. It could possibly correspond to the transition of the same energy placed earlier [3,6] as feeding into the 6_1^+ level, but the anticipated coincidence relationships would be obscured by the $\tau = 1.51(4)$ ns [40] lifetime affecting the measured transition energies as well as by poor statistics. Feeding of the 8_1^+ level, with its even longer lifetime of $\tau = 335(1)$ ns [30], could not be readily identified in the present measurements. Although the 183-keV γ ray de-exciting the isomer and the subsequent cascade were observed in the hodoscope, statistics proved insufficient to connect the decay of the long-lived state at the focal plane with prompt transitions detected by GRETINA at the target.

Figure 8 compares the ^{70}Ni levels observed solely in one-neutron knockout with the results of shell-model calculations carried out with the jj44pna effective interaction [43]. The model space included the neutron $0f_{5/2}$, $1p_{3/2}$, $1p_{1/2}$, and $0g_{9/2}$ orbitals with the requirement that a minimum of two

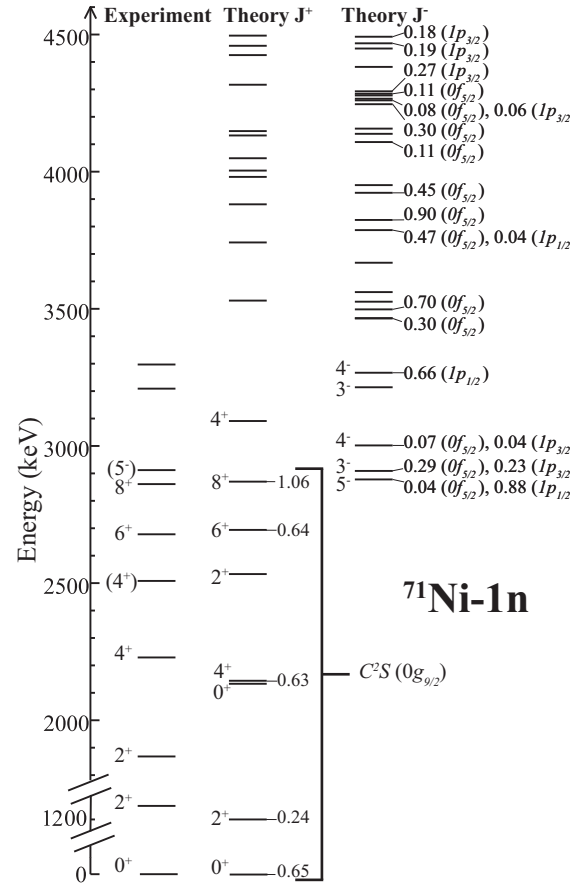

FIG. 8. Comparison of the levels populated in the one-neutron knockout reaction channel with results of shell-model calculations allowing only neutron excitations using the jj44pna effective interaction [43]. For the positive-parity states, $g_{9/2}$ shell-model spectroscopic factors C^2S for one-neutron knockout from the ^{71}Ni ground state to individual ^{70}Ni final states are listed when $C^2S(0g_{9/2}) > 0.1$. For the negative-parity levels, the $0f_{5/2}$, $1p_{3/2}$, $1p_{1/2}$ shell-model spectroscopic factors are listed when $C^2S > 0.02$ for states where the sum $C^2S(0f_{5/2}) + C^2S(1p_{3/2}) + C^2S(1p_{1/2}) > 0.1$.

neutrons occupy the $0g_{9/2}$ state. The calculated spectroscopic factors C^2S for one-neutron knockout from ^{71}Ni are listed in Fig. 8 for all levels below 4.5 MeV with $\Sigma C^2S > 0.1$. As expected, the proposed prolate structure is not reproduced as these calculations do not include cross-shell proton excitations. In addition to sizable spectroscopic strength to the 6_1^+ and 8_1^+ isomeric levels, it is clear from Fig. 8 that the anticipated strength is computed to be fragmented among many high-energy, negative-parity ^{70}Ni states. Hence, it is plausible that many of the unplaced transitions in the one-neutron channel are associated with γ decay from such negative-parity levels.

C. Two-proton knockout from ^{72}Zn

As the ^{72}Zn beam has no isomeric component, its use in two-proton knockout provides a means to confirm the role of cross-shell proton excitations without the possibility of

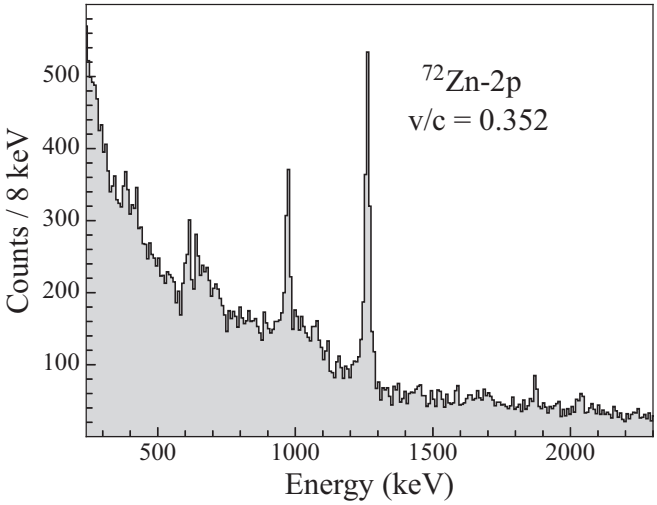

FIG. 9. Doppler-reconstructed γ-ray spectrum in coincidence with the ^{70}Ni knockout residues for the two-proton knockout from ^{72}Zn.

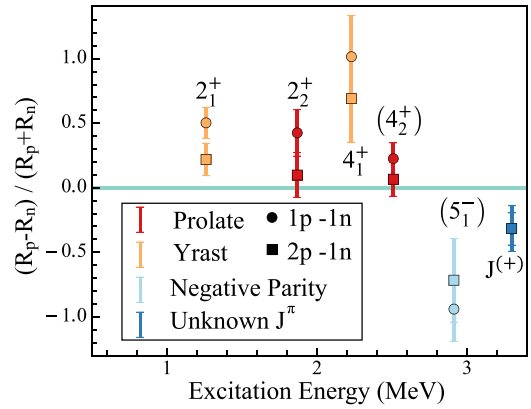

FIG. 10. Comparison of the different knockout reactions, where R_p is the ratio of the feeding-subtracted population of a state from the proton-knockout reaction channels divided by the total number of ^{70}Ni knockout residues detected for that channel, and R_n is the same for neutrons. Plotted are differences over the sums of these quantities compared to the one-neutron knockout reaction for either the one-proton (circles) or two-proton (squares) knockout cases. Points above the blue line correspond to states populated primarily in the proton-knockout reactions, while points below it would be primarily populated in the one-neutron knockout one. The state of unknown spin and parity marked as $J^{(+)}$ is the 3297-keV level.

contamination of the measured populations by knockout from isomers associated with complex configurations.

The observed Doppler-corrected γ-ray spectrum for two-proton knockout populating states in ^{70}Ni is presented in Fig. 9. As in one-proton knockout, the two-proton knockout channel predominantly populates states decaying through the yrast cascade to the ground state. The strength is largely split between the yrast levels and the proposed prolate structure, although considerably fewer transitions are observed following two-proton knockout.

As in the one-proton knockout, the 676- and 682-keV transitions could not be distinguished. Moreover, the low statistics precluded determining the intensity balance between the two γ rays based on coincidence relationships as was done in one-proton knockout and the ratio determined from the latter data was relied upon. It is possible that this approach results in an incorrect estimate for the intensity of the 676-keV γ ray as the measured intensity for the 682-keV transition combined with the assumption regarding the 676:682 ratio leads to an expected 676-keV yield below the experimental sensitivity. However, assuming the absence of any measurable 676-keV γ ray in the two-proton channel results in an increase of the 682-keV transition intensity by only 10%. In view of the small impact of this additional uncertainty on the ratio for the state populations, Table I assumes that the intensity distribution is the same in the one- and two-proton knockout channels. The adopted branching ratio from the NNDC database [30] is utilized to determine the intensity of the 234-keV transition as the peak-to-background ratio in this low-energy region of the spectrum is as poor as in one-proton knockout.

The inspection of Fig. 9 also reveals the presence of significant yield above 700 keV; i.e., close to the location of the 682-keV γ ray. This excess of counts is seen in spectra associated with two-proton knockout, as a comparison of data from the different reaction channels in Fig. 2 indicates. The shape of this "structure" could possibly be viewed as corresponding to the lineshape of a 714-keV transition emitted from a long-lived state. It could also be associated with a multiplet of unresolved, weak γ rays. In any event, the presence of this structure affects the extraction of the intensity in the 682-keV peak. For example, assuming that there is a 714-keV transition, de-exciting a level with a lifetime of the order of 75 ps leads to a decrease in the intensity of the 682-keV γ ray of 21%, as compared to that obtained if the structure is composed of prompt transitions. The errors on intensities reported in Table I for the 682-keV transition and for others depending on its yield (676 and 234 keV) reflect these difficulties.

IV. DISCUSSION

As is discussed below, the observations reported above for the relative intensities of the transitions within the proposed prolate structure are consistent with its possible proton-hole character, i.e., with the association of the states involved with the predicted prolate-deformed structure built on the (0_2^+) level [2,6].

Differences in the properties of the states fed in the three knockout reactions can be inferred from Fig. 10, where the intensity with which the states are produced in the various channels is presented as follows. First, the intensities were corrected for observed, direct feeding from other levels and they were then divided by the number of detected ^{70}Ni residues in the specific channel under consideration. Figure 10 then compares the direct population of specific states by plotting the difference of such ratios over their sum and systematically considering the proton-knockout channels versus the neutron one. In this approach, points with positive (negative) values are associated with states where larger direct population occurs via proton (neutron) knockout.

Figure 10 indicates that the proposed prolate structure and the yrast states are populated more strongly in one- and two-proton knockout reactions rather than in the one-neutron knockout channel. The difference in population in the yrast states is likely affected to some extent by a combination of factors such as the incomplete subtraction of feeding of these states through levels of negative parity populated almost exclusively in neutron knockout (see discussion above) and/or the possible presence of long-lived states in this reaction channel, which can affect the reported yields.

On the other hand, the increased population of the states proposed to be associated with excitations built on a prolate shape is noteworthy and is in line with expectations based on the predicted role of proton cross-shell excitations in the configurations of these levels. The $2_2^+ \rightarrow 0_2^+$ transition was not observed in any of the present reaction channels. Reference [6] places the (0_2^+) state at 1567 keV, resulting in a 301-keV γ ray linking the two lowest levels of the proposed prolate structure that is unlikely to compete with the higher energy $2_2^+ \rightarrow 0_1^+$ (1868 keV) and $2_2^+ \rightarrow 2_1^+$ (609 keV) transitions. Hence, the lack of observation does not appear to invalidate the proposed picture.

A similar reasoning suggests also that the stronger population of the (5^-), 2912-keV level in one-neutron knockout is consistent with the expectation that the negative-parity states are associated with neutron configurations at low excitation energy in ^{70}Ni. The placement of the 385-keV γ ray as a transition feeding the (5^-) state contradicts the work of Ref. [3], where this transition was proposed to be associated with the prolate structure. In addition, Ref. [3] had also reported a 676-keV line and had speculated that it could be part of the proposed prolate structure based on its observation in the two-neutron knockout reaction channel but absence in the deep-inelastic scattering data. The situation is more complex here: A 676-keV line is present in the one-proton knockout spectrum where it is in coincidence with the 682-keV transition, but it is not directly observed in one-neutron removal. However, as discussed above, this 676-keV energy would be compatible with that of a Doppler-reconstructed, 682-keV transition from a long-lived ($\tau \geqslant 75$ ps) state. These observations together with the noted coincidence relationships with the 682-keV, $(5^-) \rightarrow 4_1^+$ transition makes an association with the proposed proton excitations unlikely.

V. SUMMARY

The structure of the ^{70}Ni nucleus has been investigated following one-neutron and one- and two-proton knockout reactions. A number of new transitions have been added to the level scheme. Furthermore, the population of the observed levels has been found to depend on the reaction channel. Specifically, preferential population in proton knockout has been observed for a set of states proposed in earlier work to be associated with a prolate-deformed structure. The finding of preferential excitation through one- and two-proton knockout is consistent with shell-model calculations that associate this structure with proton excitations across the $Z = 28$ shell gap.

ACKNOWLEDGMENTS

This work was supported by the National Science Foundation under Grants No. PHY-1565546 and No. PHY-1811855 and by the Department of Energy, Office of Nuclear Physics, under Grants No. DE-AC02-06CH11357 (ANL), No. DE-FG02-94ER40834 (Maryland), No. DE-FG02-08ER41556 (MSU), No. DE-FG02-97ER41041 (UNC), and No. DE-FG02-97ER41033 (TUNL). This material is based upon work supported by the Department of Energy National Nuclear Security Administration through the Nuclear Science and Security Consortium under Award No. DE-NA0003180. GRETINA was funded by the DOE, Office of Science. Operation of the array at NSCL was supported by DOE under Grants No. DE-SC0014537 (NSCL) and No. DE-AC02-05CH11231 (LBNL).

[1] P. Armbruster, M. Bernas, J. P. Bocquet, R. Brissot, H. R. Faust, and P. Roussel, Europhys. Lett. **4**, 793 (1987).
[2] Y. Tsunoda, T. Otsuka, N. Shimizu, M. Honma, and Y. Utsuno, Phys. Rev. C **89**, 031301(R) (2014).
[3] C. J. Chiara, D. Weisshaar, R. V. F. Janssens, Y. Tsunoda, T. Otsuka, J. L. Harker, W. B. Walters, F. Recchia, M. Albers, M. Alcorta *et al.*, Phys. Rev. C **91**, 044309 (2015).
[4] B. P. Crider, C. J. Prokop, S. N. Liddick, M. Al-Shudifat, A. D. Ayangeakaa, M. P. Carpenter, J. J. Carroll, J. Chen, C. J. Chiara, H. M. David *et al.*, Phys. Lett. B **763**, 108 (2016).
[5] A. Morales, G. Benzoni, H. Watanabe, Y. Tsunoda, T. Otsuka, S. Nishimura, F. Browne, R. Daido, P. Doornenbal, Y. Fang *et al.*, Phys. Lett. B **765**, 328 (2017).
[6] C. J. Prokop, B. P. Crider, S. N. Liddick, A. D. Ayangeakaa, M. P. Carpenter, J. J. Carroll, J. Chen, C. J. Chiara, H. M. David, A. C. Dombos *et al.*, Phys. Rev. C **92**, 061302(R) (2015).
[7] O. Wieland, A. Bracco, F. Camera, R. Avigo, H. Baba, N. Nakatsuka, T. Aumann, S. R. Banerjee, G. Benzoni, K. Boretzky *et al.*, Phys. Rev. C **98**, 064313 (2018).
[8] R. Surman, G. C. McLaughlin, M. Ruffert, H.-T. Janka, and W. R. Hix, Astrophys. J. **679**, L117 (2008).
[9] S. N. Liddick, A. Spyrou, B. P. Crider, F. Naqvi, A. C. Larsen, M. Guttormsen, M. Mumpower, R. Surman, G. Perdikakis, D. L. Bleuel *et al.*, Phys. Rev. Lett. **116**, 242502 (2016).
[10] A. Spyrou, S. N. Liddick, F. Naqvi, B. P. Crider, A. C. Dombos, D. L. Bleuel, B. A. Brown, A. Couture, L. Crespo Campo, M. Guttormsen *et al.*, Phys. Rev. Lett. **117**, 142701 (2016).
[11] A. C. Larsen, J. E. Midtbø, M. Guttormsen, T. Renstrøm, S. N. Liddick, A. Spyrou, S. Karampagia, B. A. Brown, O. Achakovskiy, S. Kamerdzhiev *et al.*, Phys. Rev. C **97**, 054329 (2018).
[12] S. Suchyta, S. N. Liddick, Y. Tsunoda, T. Otsuka, M. B. Bennett, A. Chemey, M. Honma, N. Larson, C. J. Prokop, S. J. Quinn *et al.*, Phys. Rev. C **89**, 021301(R) (2014).

[13] S. Leoni, B. Fornal, N. Mărginean, M. Sferrazza, Y. Tsunoda, T. Otsuka, G. Bocchi, F. C. L. Crespi, A. Bracco, S. Aydin *et al.*, Phys. Rev. Lett. **118**, 162502 (2017).
[14] F. Nowacki, A. Poves, E. Caurier, and B. Bounthong, Phys. Rev. Lett. **117**, 272501 (2016).
[15] R. Taniuchi, C. Santamaria, P. Doornenbal, A. Obertelli, K. Yoneda, G. Authelet, H. Baba, D. Calvet, F. Château, A. Corsi *et al.*, Nature (London) **569**, 53 (2019).
[16] A. Gade and S. N. Liddick, J. Phys. G **43**, 024001 (2016).
[17] D. Pauwels, O. Ivanov, N. Bree, J. Büscher, T. E. Cocolios, J. Gentens, M. Huyse, A. Korgul, Y. Kudryavtsev, R. Raabe *et al.*, Phys. Rev. C **78**, 041307(R) (2008).
[18] A. Gade, R. V. F. Janssens, D. Bazin, R. Broda, B. A. Brown, C. M. Campbell, M. P. Carpenter, J. M. Cook, A. N. Deacon, D.-C. Dinca *et al.*, Phys. Rev. C **74**, 021302(R) (2006).
[19] M. Schramm, K. H. Maier, M. Rejmund, L. D. Wood, N. Roy, A. Kuhnert, A. Aprahamian, J. Becker, M. Brinkman, D. J. Decman *et al.*, Phys. Rev. C **56**, 1320 (1997).
[20] M. Petri, P. Fallon, A. O. Macchiavelli, S. Heil, E. Rodriguez-Vieitez, D. Bazin, C. M. Campbell, R. M. Clark, M. Cromaz, A. Gade *et al.*, Phys. Lett. B **748**, 173 (2015).
[21] A. Gade, J. A. Tostevin, V. Bader, T. Baugher, D. Bazin, J. S. Berryman, B. A. Brown, C. A. Diget, T. Glasmacher, D. J. Hartley *et al.*, Phys. Rev. C **93**, 054315 (2016).
[22] A. Gade and B. M. Sherrill, Phys. Scr. **91**, 053003 (2016).
[23] D. Morrissey, B. Sherrill, M. Steiner, A. Stolz, and I. Wiedenhoever, Nucl. Instrum. Methods Phys. Res. B **204**, 90 (2003).
[24] D. Bazin, J. Caggiano, B. Sherrill, J. Yurkon, and A. Zeller, Nucl. Instrum. Methods Phys. Res. B **204**, 629 (2003).
[25] J. Yurkon, D. Bazin, W. Benenson, D. Morrissey, B. Sherrill, D. Swan, and R. Swanson, Nucl. Instrum. Methods Phys. Res. A **422**, 291 (1999).
[26] S. Paschalis, I. Lee, A. Macchiavelli, C. Campbell, M. Cromaz, S. Gros, J. Pavan, J. Qian, R. Clark, H. Crawford *et al.*, Nucl. Instrum. Methods Phys. Res. A **709**, 44 (2013).
[27] D. Weisshaar, D. Bazin, P. C. Bender, C. M. Campbell, F. Recchia, V. Bader, T. Baugher, J. Belarge, M. P. Carpenter, H. L. Crawford *et al.*, Nucl. Instrum. Methods Phys. Res. A **847**, 187 (2017).
[28] K. Meierbachtol, D. Bazin, and D. Morrissey, Nucl. Instrum. Methods Phys. Res. A **652**, 668 (2011).
[29] K. Wimmer, D. Barofsky, D. Bazin, L. Fraile, J. Lloyd, J. Tompkins, and S. Williams, Nucl. Instrum. Methods Phys. Res. A **769**, 65 (2015).
[30] Evaluated nuclear structure data file (ensdf) [http://www.nndc.bnl.gov/ensdf].
[31] I. Stefanescu, D. Pauwels, N. Bree, T. E. Cocolios, J. Diriken, S. Franchoo, M. Huyse, O. Ivanov, Y. Kudryavtsev, N. Patronis *et al.*, Phys. Rev. C **79**, 044325 (2009).
[32] P. Hansen and J. Tostevin, Annu. Rev. Nucl. Part. Sci. **53**, 219 (2003).
[33] F. Recchia, D. Weisshaar, A. Gade, J. A. Tostevin, R. V. F. Janssens, M. Albers, V. M. Bader, T. Baugher, D. Bazin, J. S. Berryman *et al.*, Phys. Rev. C **94**, 054324 (2016).
[34] A. Gade and T. Glasmacher, Prog. Part. Nucl. Phys. **60** (2008).
[35] UCGretina GEANT4, L. A. Riley, Ursinus College (unpublished).
[36] C. Loelius, H. Iwasaki, B. A. Brown, M. Honma, V. M. Bader, T. Baugher, D. Bazin, J. S. Berryman, T. Braunroth, C. M. Campbell *et al.*, Phys. Rev. C **94**, 024340 (2016).
[37] G. Mairle, G. Kaschl, H. Link, H. Mackh, U. Schmidt-Rohr, G. Wagner, and P. Turek, Nuc. Phys. A **134**, 180 (1969).
[38] M. Sawicka, R. Grzywacz, I. Matea, H. Grawe, M. Pfützner, J. M. Daugas, M. Lewitowicz, D. L. Balabanski, F. Becker, G. Bélier *et al.*, Phys. Rev. C **68**, 044304 (2003).
[39] W. F. Mueller, B. Bruyneel, S. Franchoo, M. Huyse, J. Kurpeta, K. Kruglov, Y. Kudryavtsev, N. V. S. V. Prasad, R. Raabe, I. Reusen *et al.*, Phys. Rev. C **61**, 054308 (2000).
[40] H. Mach, M. Lewitowicz, M. Stanoiu, F. Becker, J. Blomqvist, M. Berge, R. Boutami, B. Cederwall, Z. Dlouhy, B. Fogelberg *et al.*, Nuc. Phys. A **719**, C213 (2003).
[41] C. J. Prokop, Ph.D. thesis, Michigan State University, East Lansing, MI, 2016 (unpublished).
[42] A. Gade, R. V. F. Janssens, J. A. Tostevin, D. Bazin, J. Belarge, P. C. Bender, S. Bottoni, M. P. Carpenter, B. Elman, S. J. Freeman *et al.*, Phys. Rev. C **99**, 011301(R) (2019).
[43] A. F. Lisetskiy, B. A. Brown, M. Horoi, and H. Grawe, Phys. Rev. C **70**, 044314 (2004).